JOURNAL OF SOLID STATE CHEMISTRY 117, 39–47 (1995)

Preparation, Structure Determination and Thermal Transformation of a New Lithium Zinc Phosphate, δ_1-$LiZnPO_4$

Torben R. Jensen, Poul Norby,[1] and Paul C. Stein

Department of Chemistry, University of Odense, DK-5230 Odense, Denmark

and

Anthony M. T. Bell

SERC Daresbury Laboratory, Cheshire WA4 4AD, England

Received May 2, 1994; in revised form November 14, 1994; accepted November 16, 1994

A new lithium zinc orthophosphate, δ_I-$LiZnPO_4$, was synthesized from aqueous solution. Information from powder diffraction, using synchrotron radiation, and ^{31}P MAS NMR spectroscopy allowed determination of the structure. The structure is orthorhombic (a = 10.0193(1), b = 4.9657(1), c = 6.6746(1) Å), space group $Pna2_1$, No. 33, Z = 4. The structure may be seen as built from corner-sharing ZnO_4- and PO_4- tetrahedra forming a cristobalite-type framework structure. The lithium ions are 4-coordinated and situated in the 6-ring channels. The thermal transformations were investigated by thermogravimetric measurements (TG), differential thermal analysis (DTA), and high-temperature powder diffraction (HT-PXD). A transformation at ~575°C is clearly visible on the Guinier Simon film (HT-PXD). This transformation is characterized by some disappearing lines in the powder pattern. The high-temperature polymorph of δ_I-$LiZnPO_4$ is named δ_{II}-$LiZnPO_4$. Phase transformations at ~730 and ~1003°C are observed by HT-PXD and DTA, respectively. These observations are designated to the transformation to β-$LiZnPO_4$ and from β- to γ-$LiZnPO_4$.

INTRODUCTION

Crystalline lithium compounds have been extensively studied due to the interest in Li ion-conducting solid electrolytes for lithium batteries. A large number of zeolite-like phosphates have been synthesized, e.g., aluminophosphates, which have neutral frameworks as opposed to the anionic aluminosilicates. By substituting the trivalent aluminium with a divalent framework ion and a monovalent counterion, e.g., $Al^{3+} \rightarrow Li^+ + Zn^{2+}$, materials with potential ion exchange and ion conduction properties may be obtained.

[1] To whom correspondence should be addressed at present address: Chemistry Department, Brookhaven National Laboratory, Upton, New York 11973.

$LiZnPO_4 \cdot H_2O$ was recently synthesized by Gier and Stucky (1) from an aqueous solution at 70°C, pH 7. The structure was proposed to be similar to the zeolite structure type ABW.

The phase diagram of the system Li_3PO_4-$Zn_3(PO_4)_2$ has been investigated by Torres-Trevino and West (2) by means of solid state reactions and thermal analysis. A number of new phases were observed. The transition temperatures of α-, β-, and γ-$LiZnPO_4$ and the monoclinic unit cell parameters of α-$LiZnPO_4$ were determined (2). The structure of α-$LiZnPO_4$ has been solved by Elammari and Elouadi (3).

We report here the crystal structure and thermal transformations of a new lithium zinc phosphate, δ_I-$LiZnPO_4$, synthesized from an aqueous solution. The structure was solved from synchrotron powder diffraction data and ^{31}P MAS NMR. The thermal transformations were investigated by thermogravimetric measurements (TG), differential thermal analysis (DTA), and high-temperature powder diffraction (HT-PXD).

EXPERIMENTAL

Sample Preparation

The materials used in this study were synthesized from LiOH (Merck, >98%), Zn (Merck, pro analysi), HNO_3 (Ferak, zur analyse, >65%), H_3PO_4 (Union Carbide, Fluka, puriss p.a., 85%) and $Zn(NO_3)_2 \cdot 6H_2O$ (Union Carbide, Fluka, purum p.a.).

LiOH (1.300 g) was dissolved in 25 ml H_2O. Powdered Zn (0.806 g) was dissolved in 3 ml conc. HNO_3, 5 ml H_2O, and 0.9 ml H_3PO_4. The two solutions were mixed in a Pyrex Erlen Meyer flask under stirring. The sealed flask was placed at ~95°C for 48 hr. The product contained an impurity of β-Li_3PO_4. It was found that formation of β-

0022-4596/95 $6.00

TABLE 1
Indexed Synchrotron X Ray Powder Pattern for δ_I-$LiZnPO_4$

h	k	l	d_{calc}	d_{obs}	Int.	h	k	l	d_{calc}	d_{obs}	Int.
2	0	0	5.0097	5.0127	3	2	3	1	1.5298	1.5300	1
2	0	1	4.0066	4.0090	100	5	2	1	1.5185	1.5185	1
0	1	1	3.9841	3.9847	92	2	1	0	1.5083	1.5084	4
1	1	1	3.7021	3.7037	13	6	0	2	1.4934	1.4934	14
2	1	0	3.5267	3.5275	7	3	3	0	1.4831	1.4836	5
0	0	2	3.3373	3.3380	4	1	3	2	1.4669	1.4670	9
2	1	1	3.1182	3.1194	13	3	3	1	1.4478	1.4480	3
2	0	2	2.7774	2.7779	35	6	1	2	1.4301	1.4301	3
1	1	2	2.6697	2.6700	18	5	1	3	1.4262	1.4263	1
3	1	1	2.5594	2.5602	6	2	3	2	1.4219	1.4221	1
4	0	0	2.5048	2.5054	31	5	2	2	1.4127	1.4129	3
0	2	0	2.4828	2.4837	33	4	0	4	1.3887	1.3886	5
2	1	2	2.4240	2.4240	15	0	2	4	1.3849	1.3850	5
1	2	0	2.4099	2.4109	3	4	2	3	1.3819	1.3822	2
4	0	1	2.3451	2.3458	5	7	1	0	1.3753	1.3754	1
1	2	1	2.2667	2.2670	3	1	2	4	1.3719	1.3720	3
4	1	0	2.2364	2.2369	2	3	3	2	1.3553	1.3554	9
2	2	0	2.2246	2.2252	1	7	1	1	1.3470	1.3472	1
3	1	2	2.1320	2.1325	11	4	1	4	1.3374	1.3374	3
4	1	1	2.1205	2.1207	9	6	0	3	1.3355	1.3356	2
2	2	1	2.1105	2.1109	9	0	3	3	1.3280	1.3280	1
2	0	3	2.0334	2.0322	9	1	3	3	1.3165	1.3166	4
4	0	2	2.0033	2.0035	3	6	1	3	1.2897	1.2896	10
0	2	2	1.9920	1.9910	6	2	3	3	1.2837	1.2833	2
1	2	2	1.9538	1.9540	3	6	2	2	1.2797	1.2798	7
3	2	1	1.9093	1.9094	5	5	3	0	1.2762	1.2764	2
2	1	3	1.8817	1.8817	7	7	1	2	1.2716	1.2719	1
5	1	0	1.8583	1.8582	4	5	3	1	1.2535	1.2534	2
2	2	2	1.8511	1.8512	9	2	1	5	1.2485	1.2485	1
5	1	1	1.7902	1.7903	2	5	1	4	1.2416	1.2415	1
4	2	0	1.7634	1.7636	6	3	3	3	1.2340	1.2341	2
3	1	3	1.7349	1.7348	2	1	4	0	1.2320	1.2317	2
4	2	1	1.7049	1.7050	2	7	2	1	1.2192	1.2192	1
0	0	4	1.6686	1.6687	13	8	1	0	1.2144	1.2144	2
4	0	3	1.6634	1.6636	5	4	2	4	1.2120	1.2119	3
1	2	3	1.6347	1.6347	2	3	1	5	1.2027	1.2026	1
5	1	2	1.6235	1.6235	2	8	1	1	1.1948	1.1948	1
6	0	1	1.6199	1.6201	3	5	3	2	1.1920	1.1922	1
0	3	1	1.6066	1.6066	3	2	4	1	1.1858	1.1859	1
1	3	1	1.5863	1.5863	4	4	0	5	1.1781	1.1779	1
4	1	3	1.5773	1.5773	3	6	2	3	1.1762	1.1762	1
2	2	3	1.5731	1.5731	3	7	1	3	1.1699	1.1697	1
4	2	2	1.5591	1.5592	3	1	2	5	1.1677	1.1678	1
6	1	1	1.5401	1.5402	4	0	4	2	1.1635	1.1635	1

TABLE 1—*Continued*

h	k	l	d_{calc}	d_{obs}	Int.	h	k	l	d_{calc}	d_{obs}	Int.
6	3	1	1.1577	1.1579	1	2	5	2	0.9352	0.9352	1
1	4	2	1.1558	1.1558	1	1	1	7	0.9323	0.9323	1
4	1	5	1.1462	1.1462	3	7	4	1	0.9287	0.9288	1
2	2	5	1.1446	1.1447	2	6	0	6	0.9258	0.9257	1
5	2	4	1.1393	1.1393	1	9	3	0	0.9238	0.9239	1
3	3	4	1.1085	1.1086	2	5	3	5	0.9225	0.9226	1
5	3	3	1.1070	1.1072	2	10	2	1	0.9203	0.9203	1
8	2	1	1.1028	1.1029	1	1	3	6	0.9194	0.9194	1
3	4	2	1.0988	1.0988	1	3	5	2	0.9154	0.9154	2
4	4	1	1.0972	1.0974	1	8	0	5	0.9134	0.9134	1
8	0	3	1.0914	1.0914	2	6	1	6	0.9101	0.9101	1
2	0	6	1.0860	1.0861	1	7	3	4	0.9082	0.9082	2
7	3	0	1.0827	1.0829	2	5	2	6	0.9056	0.9055	1
1	4	3	1.0778	1.0778	2	1	5	3	0.9032	0.9032	1
7	3	1	1.0687	1.0688	1	10	1	3	0.8985	0.8984	1
4	2	5	1.0643	1.0642	1	10	2	2	0.8951	0.8951	1
2	1	6	1.0609	1.0609	3	5	4	4	0.8919	0.8920	1
5	4	0	1.0553	1.0554	1	3	3	6	0.8899	0.8899	1
6	0	5	1.0427	1.0426	1	1	2	7	0.8866	0.8867	1
6	3	3	1.0394	1.0393	1	6	3	5	0.8822	0.8822	1
9	1	2	1.0329	1.0332	1	4	1	7	0.8771	0.8771	1
3	4	3	1.0311	1.0311	2	3	5	3	0.8752	0.8752	1
7	3	2	1.0298	1.0299	1	6	2	6	0.8675	0.8675	1
6	1	5	1.0204	1.0204	1	3	2	7	0.8601	0.8601	1
5	3	4	1.0137	1.0137	1	10	3	0	0.8571	0.8571	1
1	2	6	1.0100	1.0100	1	9	3	3	0.8531	0.8532	1
5	4	2	1.0062	1.0062	1	7	3	5	0.8409	0.8409	1
9	2	1	1.0042	1.0043	1	5	3	6	0.8386	0.8385	1
8	2	3	0.9991	0.9991	1	12	0	0	0.8349	0.8350	1
0	4	4	0.9960	0.9957	1	0	0	8	0.8343	0.8344	1
1	4	4	0.9911	0.9912	2	5	4	5	0.8279	0.8279	1
8	1	4	0.9819	0.9819	3	1	3	7	0.8234	0.8234	1
1	5	1	0.9776	0.9778	1	6	1	7	0.8168	0.8168	1
7	3	3	0.9735	0.9733	1	10	2	4	0.8118	0.8118	1
9	2	2	0.9718	0.9718	1	2	6	1	0.8105	0.8105	1
4	3	5	0.9598	0.9597	1	9	3	4	0.8082	0.8081	1
3	4	4	0.9545	0.9545	1	9	4	2	0.8044	0.8044	1
3	5	0	0.9519	0.9520	1	11	3	0	0.7980	0.7979	1
1	5	2	0.9476	0.9477	1	7	5	2	0.7926	0.7925	1
10	1	2	0.9422	0.9423	1	10	1	5	0.7911	0.7911	1
2	0	7	0.9367	0.9366	1	12	0	3	0.7817	0.7817	1

Note. Indexing based on an orthorhombic unit cell: a = 10.0193(1), b = 4.9657(1), c = 6.6746(1) Å. Volume = 332.08(1) Å^3.

Li_3PO_4 could be suppressed by lowering pH. The material for powder diffraction using neutron radiation was synthesized in a similar way.

The temperature of the two solutions, when mixing, seems to be important for the obtained product. Phase pure δ_I-$LiZnPO_4$ is obtained by mixing hot solutions. This suppress formation of $LiZnPO_4 \cdot H_2O$, which forms in the same pH range as δ_I-$LiZnPO_4$, but at lower temperatures, was prepared according to Ref. (1). By heating $LiZnPO_4 \cdot H_2O$ dry or hydrothermal it transforms to δ_I-$LiZnPO_4$ (4).

Characterization

Powder diffraction data for determining and refining unit cell parameters were obtained, using a Siemens D5000 powder diffractometer, equipped with a primary Ge-monochromator (Cu$K\alpha_1$ radiation, λ = 1.540598 Å). The data were collected from 10° to 90° in 2θ, with a steplength of 0.02°, and counting time of 12 sec per step, using a flat sample. The trial and error indexing program TREOR (5) was used in determining the unit cell parameters, and the CELLKANT (6) program was used to refine the unit cell parameters from the observed d-spacings.

TABLE 2

Weak Lines Which Could Be Indexed with a Unit Cell Identical to β-Li_3PO_4: a = 6.119(4), b = 5.238(3), c = 4.882(4) Å. Volume = 156.5(2) Å^3

h	k	l	d_{calc}	d_{obs}	Int.	h	k	l	d_{calc}	d_{obs}	Int.
0	1	0	5.2382	5.2429	2	2	1	0	2.6420	2.6435	2
1	0	1	3.8162	3.8164	2	0	2	0	2.6191	2.6225	1
0	1	1	3.5713	3.5741	2	0	0	2	2.4409	2.4412	2
1	1	1	3.0845	3.0867	1	2	1	1	2.3236	2.3208	1
2	0	0	3.0597	3.0612	1	0	3	1	1.6441	1.6430	1

The refinement using CELLKANT showed that the b axis, proposed by TREOR, could be bisected.

Synchrotron X-ray powder diffraction data were collected using the high-resolution powder diffractometer on the station 2.3 (7, 8) of the UK Synchrotron Radiation Source at Daresbury Laboratory. Data were collected from 13.5° to 113.5° in 2θ, at a wavelength of 1.2999 Å, using a steplength of 0.01°. The wavelength was calibrated from a data set collected on an NBS (640b) silicon standard. The wavelength is above (approximately 125 eV) the absorption edge of Zn (1.283 Å (9)). Data were collected with a fixed counting time (2 sec per step), using a scintillation detector. The data were afterward scaled using monitor counts. A small range (46.50°–46.56° in 2θ) of the diagram was excluded from the calculations, due to refilling of the storage ring. The data were recorded using a flat sample, which was rotated to reduce the effect of preferred orientation.

The indexed synchrotron powder diagram (170 reflections) is provided in Table 1. The refined unit cell dimensions are a = 10.0193(1), b = 4.9657(1), c = 6.6746(1) Å. In addition 10 weak reflections ($I/I_0 < 2\%$) were observed, which could not be indexed using this unit cell. Trial and error indexing with TREOR (5) suggested another unit cell (a = 6.119(4), b = 5.238(3), and c = 4.882(4) Å), which matches that of β-Li_3PO_4 (10). The indexed weak reflections are provided in Table 2.

Neutron radiation powder diffraction data were collected from 10.0° to 115.7° in 2θ, with a steplength of 0.053°, using the instrument at Risø National Laboratory, Denmark; for further experimental details, see Ref. (11). The wavelength was 1.43714 Å.

Structure factors were extracted from the synchrotron powder diagram with the deconvolution program ALLHKL (12). The extracted structure factors were used in direct methods calculations, using the program SHELXS-86 (13). Difference Fourier calculations were performed with the program XRS-82 (14). The program system XRS-82 was also used for the structure refinements, using the Rietveld full-profile method, as well as geometric refinement (distance angle least squares, DALS). The program FPRIME (15) was used to calculate the resonant scattering contribution.

^{31}P MAS NMR spectra were recorded on a Varian UNITY-500 spectrometer (11.7 T, $\nu(^{31}P)$ = 202 MHz). The high-speed MAS probe was built at the University of Aarhus, Denmark (16). Cylindrical rotors (5 mm o.d., Si_3N_4) with a sample volume of 220 μl and a maximum spinning speed of 15 kHz were used. The reference was 85% H_3PO_4 (Union Carbide, Fluka, puriss p.a.).

Infrared spectra were recorded on a Perkin–Elmer 1720 Fourier transform spectrograph using pellets of KBr containing 1% of the compounds. Spectral resolution was 4 cm^{-1}.

Thermogravimetric measurements were performed between RT and 950°C, using a SETARAM TG 92-12 instrument and Al_2O_3 crucibles as sample holders (N_2 atmosphere); heating rate was 5°C/min. High-temperature powder diffraction data were collected between RT and 965°C, using an Enraf-Nonius Guinier Simon camera ($CuK\alpha_1$ radiation), with the movement of the film cassette being synchronized with the change in temperature; heating rate ~1°C/min. The samples were kept in open quartz capillaries. Differential thermal analysis measurements were carried out between RT and 1150°C, using Al_2O_3 crucibles as sample holders, and Al_2O_3 as reference (N_2 atmosphere); heating rate 10°C/min. The instrument was a Netzsch 404EP thermoanalyzer, calibrated with antimony (mp 630.7°C). Thermal analyses (DTA and HT-PXD) were performed at the University of Oslo, Norway.

RESULTS AND DISCUSSION

Structure Determination

The first step required in the process of solving a crystal structure is to determine the unit cell and the correct space group. The systematic extinctions were in agreement with two possible extinction symbols *Pn*– (*Pnm*2_1, *Pnmm*, and *Pn*2_1*m*) and *Pna*- (*Pna*2_1 and *Pnam*). Ignoring a few weak reflections ($I/I_0 < 5\%$) makes the extinction symbol, *Pn-a* (*Pn*2_1*a* and *Pnma*), compatible with the systematically absent reflections.

In order to determine the correct extinction symbol, the calculated peak width functions (assuming a pseudo-Voigt peak shape) were investigated. The full-width at half-maximum (FWHM) of the diffraction peaks may be described as a function of θ, defined by three variables U, V, and W, using

$$\mathrm{FWHM}(\theta) = [U \tan^2(\theta) + V \tan(\theta) + W]^{1/2}.$$

To verify the extinction symbols suggested by indexing, profile refinements using ALLHKL (12) were performed with no systematic extinctions, *P*---, and with systematic

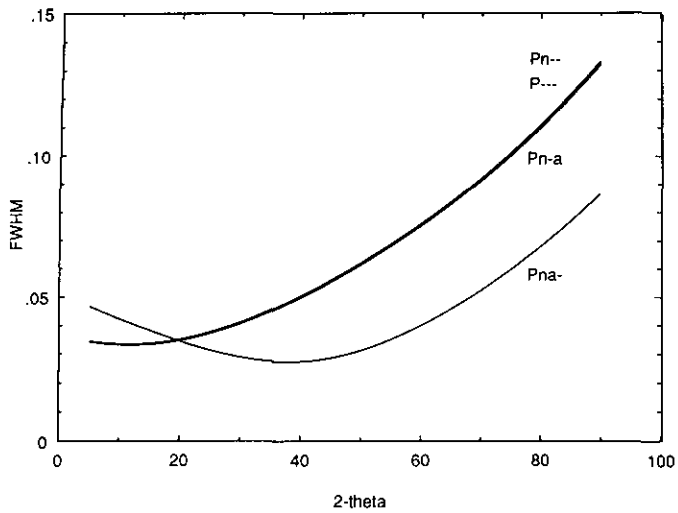

FIG. 1. Full-width at half-maximum (FWHM) functions calculated by profile refinement using the program ALLHKL (12) and the extinction symbols: *P*---, *Pn*--, *Pna*-, and *Pn-a*.

extinctions, as given by the extinction symbols *Pn*--, *Pna*-, and *Pn-a*. The half-width functions are plotted in Fig. 1. The half-width function obtained using *Pna*- differs clearly from those using *P*---, *Pn*--, and *Pn-a*, which may indicate that *Pna*- is indeed the correct solution. Thus, two space-groups, $Pna2_1$ and *Pnam*, were considered.

Comparing half-width functions in order to suggest the correct extinction symbol is not an universally applicable technique. However, when using powder diffraction a reliable determination of systematic extinctions is often not easily derived due to overlapping reflections. In order to determine the correct extinction symbol, a closer examination of the half-width functions may prove useful.

^{31}P MAS NMR spectroscopy indicated one phosphorus atom in the asymmetric unit and an ordered Li/Zn distribution. Table 3 provides chemical shift, $\delta(^{31}P)$, and the FWHM of the peaks of some selected compounds. Chemical shifts, $\delta(^{31}P)$, of the compounds δ_I-$LiZnPO_4$ and $LiZnPO_4 \cdot H_2O$ are different. The IR-spectra of δ_I-$LiZnPO_4$ showed that the compound contained no crystal water,

TABLE 3

^{31}P MAS NMR Chemical Shifts and Full-Width at Half-Maximum (FWHM) of Selected Compounds

Compound	δ (ppm)	FWHM (Hz)
δ_I-$LiZnPO_4$	11.39	81
$LiZnPO_4 \cdot H_2O$	6.12	99
β-Li_3PO_4	10.60	306
H_3PO_4 (85%)	0	43

Note. The spectral resolution was 5 Hz (digital resolution 1.24 Hz), which compares to an accuracy of 0.02 ppm on chemical shift. Reference: H_3PO_4 (85%).

and the performed thermogravimetric measurements showed no weight loss.

Solving structures from powder data is often time consuming, and it is often valuable to look for related compounds. In this case the anhydrous zeolite Li–*A*(*BW*), $LiAlSiO_4$ (17), and δ_I-$LiZnPO_4$ have similar unit cells, which might suggest that the structures of the two compounds are related. Geometric refinement of the *ABW* structure into the found unit cell (space group $Pn2_1b$), using the program system XRS-82 (14) and starting coordinates from the structure of zeolite Li–*A*(*BW*) (17), provided a new set of coordinates. However, subsequent Rietveld refinement showed that the *ABW* structure was not compatible with the observed diagram.

Individual structure factors were extracted from the synchrotron powder diagram by deconvolution, using the ALLHKL program (12). A set of 184 structure factors were used in the subsequent determination of the structure by direct methods. Direct methods using SHELXS-86 (13) (in $Pna2_1$) provided the positions of phosphorus, zinc, and two oxygens. The two additional oxygen atoms were located by difference Fourier calculations using the program system XRS-82 (14). The structure (Zn, P, and O(1)–O(4)) was geometrically refined using constraints on the bond lengths and the angles in the tetrahedra. Difference Fourier calculations then revealed the lithium position.

The population parameter of Zn and Li refined to $PP_{Zn} = 0.8$ and $PP_{Li} = 1.5$. The wavelength used is close to the absorption edge of Zn and resonant scattering effects are significant. In order to determine if the discrepancies found for the population parameters was due to resonant scattering, the program FPRIME (15) was used to estimate f' and f'', giving values at -4.021 and 0.498, respectively. Introduction of f' and f'' in the refinement resulted in more consistent population parameters, $PP_{Zn} = 0.925(3)$ and $PP_{Li} = 1.47(2)$.

The final refinement of the structure was performed using the program XRS-82 (14) using the Rietveld full-profile method. The observed, calculated, and different profiles after the final refinement are shown in Fig. 2. Structural parameters and *R* values are given in Table 4 and interatomic distances and angles are listed in Table 5.

Rietveld refinement using data obtained with conventional X-ray radiation resulted in $PP_{Zn} = 0.899(7)$ and $PP_{Li} = 1.75(5)$. The temperature factor of zinc refined to $B_{Zn} = 0.56(7)$ Å^2.

The structural parameters refined with the neutron radiation data were in agreement with the results represented in Table 4. In agreement with the synchrotron X-ray refinement, this refinement revealed only one lithium position in the structure. The refinement with neutron data proposed also the possibility of a slightly disordered Li/Zn distribution. However, due to low quality of the neu-

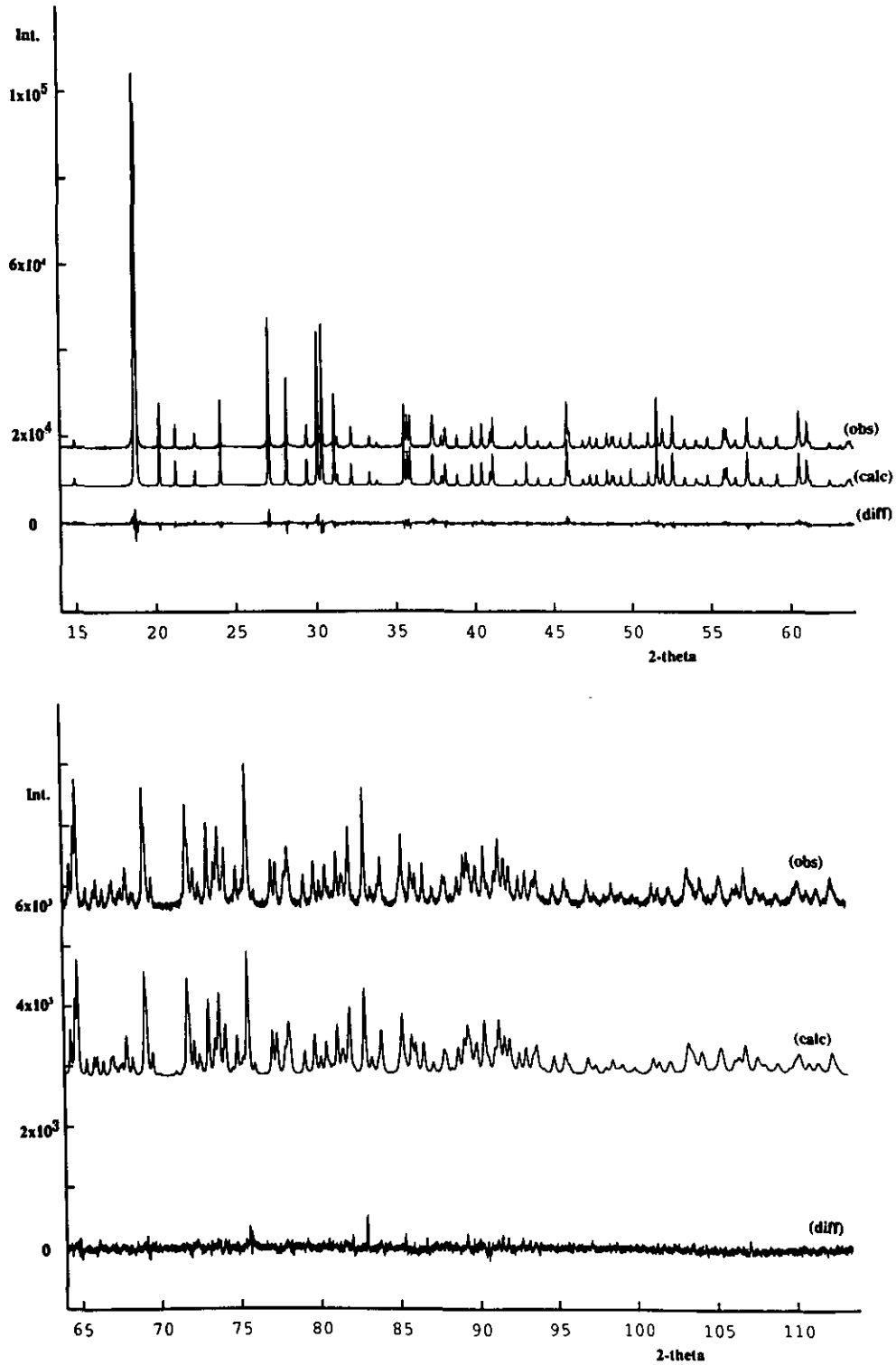

FIG. 2. Observed, calculated, and difference synchrotron X-ray powder diffraction profiles.

tron data, it was not possible to perform acceptable profile refinements.

The refinements, with different data sets, suggest an almost ordered distribution of Li and Zn. From the population parameter, PP_{Zn} (Table 4), a content of Li on the Zn position may be estimated to 8%. Likewise, the high occupancy of lithium may be explained by a content of approximately 5% Zn on this position. The refined popula-

TABLE 4
Refined Atomic Coordinates and Isotropic Temperature Factors, Standard Deviation in Parentheses

Atom	x	y	z	B_{iso} (Å^2)	PP	V_i
Zn	0.8449(1)	0.1870(1)	0[a]	0.51(3)	0.925(3)[b]	2.02
Li	0.1569(6)	0.825(1)	0.989(4)	1.7(3)	1.47(2)[c]	1.02
P	0.0926(1)	0.3164(3)	0.7504(6)	0.32(3)		5.01
O(1)	0.9439(3)	0.2455(6)	0.757(1)	0.5(1)		2.06
O(2)	0.8863(3)	0.3849(6)	0.2528(9)	0.9(1)		2.11
O(3)	0.3389(4)	0.6996(6)	0.4401(7)	0.3(1)		2.00
O(4)	0.3396(3)	0.6965(6)	0.0552(8)	0.3(1)		1.89

Number of contributing reflections 386
Number of variables 38
R factors (%) $R_F = 4.7$
$R_I = 7.9$
$R_P = 11.7$
$R_{wP} = 11.1$
$R_E = 6.0$ (statistically expected)
$R_{wS} = 4.0$ (soft restrictions)

Note. Bond valences, V_i, were calculated according to Ref. (18). The Li/Zn distribution was not included in the bond valences calculations.
[a] Kept constant to define zero point.
[b] ~92% Zn, 8% Li.
[c] ~92% Li, 8% Zn.

TABLE 5
Interatomic Distances (Å) and Angles (°) in the δ_I-$LiZnPO_4$ Structure, Standard Deviation in Parentheses

Distances		Angles		
Zn–O(1)	1.925(6)	O(1)–Zn–O(2)		122.1(2)
O(2)	1.996(5)	O(1)	O(3)	105.6(2)
O(3)	1.967(4)	O(1)	O(4)	109.2(2)
O(4)	1.942(3)	O(2)	O(3)	103.0(2)
Mean	1.958	O(2)	O(4)	108.8(2)
		O(3)	O(4)	107.1(1)
Li–O(1)	2.09(2)	O(1)–Li–O(2)		119.9(3)
O(2)	1.94(2)	O(1)	O(3)	108.9(8)
O(3)	1.89(1)	O(1)	O(4)	101.1(9)
O(4)	1.99(1)	O(2)	O(3)	113(1)
Mean	1.98	O(2)	O(4)	102.7(6)
		O(3)	O(4)	109.6(3)
P–O(1)	1.531(3)	O(1)–P–O(2)		111.4(2)
O(2)	1.499(3)	O(1)	O(3)	108.8(3)
O(3)	1.553(6)	O(1)	O(4)	110.9(3)
O(4)	1.575(6)	O(2)	O(3)	107.4(3)
Mean	1.540	O(2)	O(4)	108.8(3)
		O(3)	O(4)	109.5(2)
Zn–O(1)–P	124.1(4)	Zn–O(2)–P		120.5(4)
Zn Li	116.7(4)	Zn	Li	112.0(5)
P Li	119.1(5)	P	Li	125.0(6)
Zn–O(3)–P	118.2(2)	Zn–O(4)–P		121.3(2)
Zn Li	105.5(3)	Zn	Li	107.2(3)
P Li	119.9(7)	P	Li	117.7(6)

tion parameters are, however, correlated with the temperature factors, and care should be taken when evaluating population parameters. When the population parameters were fixed at 1.0, the temperature factors refined to B_{Zn} = 0.73(7) and $B_{Li} = -13.5(6)$ Å^2 (the temperature factors of the other atoms in the structure were fixed at $B = 0.6$ Å^2), using the synchrotron X-ray data.

When looking at the coordinates (Table 4) it is seen that the structure is very close to having *Pnam* symmetry, with a mirror plane perpendicular to the c axis. Thus, P, O(1), and O(2) would be on the mirror plane, while Li and Zn would be symmetry related, together with O(3) and O(4). This would mean that Li and Zn was statistically distributed. However, refinement in this space group clearly showed that Li and Zn are not statistically distributed, and the true space group is $Pna2_1$. The apparent pseudo-mirror plane is present because the Li–O and Zn–O distances are very similar.

Tables 4 and 5 show that the PO_4^- tetrahedra is regular, whereas the ZnO_4^- and LiO_4^- tetrahedra are slightly distorted. The mean interatomic distances are in good agreement with the results by Elammari and Elouadi on the structure of α-$LiZnPO_4$ (3). The bond valences, V_i, are calculated according to Brown and Altermatt (18). The Li/Zn distribution was not included in the calculations, as the geometry of the structure is not likely to be perturbed by the disorder. (The disorder is small, and the Li–O and Zn–O distances are almost identical.) The bond valences, V_i, are in good agreement with the expected oxidation states of the ions.

Structure Description

The structure of this new lithium zinc phosphate, δ_I-$LiZnPO_4$, can be viewed as a 3-dimensional framework built from cornersharing ZnO_4^- and PO_4^- tetrahedra, with 4-coordinated Li in interstitial positions. Figures 3a and 3b show that this framework is of cristobalite type. Figure 3a show that chains of alternating cornersharing ZnO_4 and PO_4 tetrahedra are running in the direction of the a axis. δ_I-$LiZnPO_4$ may, thus, be described as a stuffed derivative of cristobalite similar to, e.g., high-carnegeite, $NaAlSiO_4$ (19), and γ-eucryptite, $LiAlSiO_4$ (17). γ-eucryptite, $LiAlSiO_4$, is formed by heating the zeolite Li-$A(BW)$, $LiAlSiO_4 \cdot H_2O$ (17). The cristobalite structure can be described as built from hexagonal nets (stacking sequence ABC) of corner-sharing tetrahedra with apexes pointing alternating up and down (UDUDUD). The pseudo-hexagonal net in the structure of δ_I-$LiZnPO_4$ is shown in Fig. 3b.

The structure could equally well be seen as built from PO_4^- and LiO_4^- tetrahedra forming a cristobalite-type framework with zinc in tetrahedral sites. All the tetrahedra are corner sharing, resulting in three coordinated oxygen in contact with phosphor, zinc, and lithium.

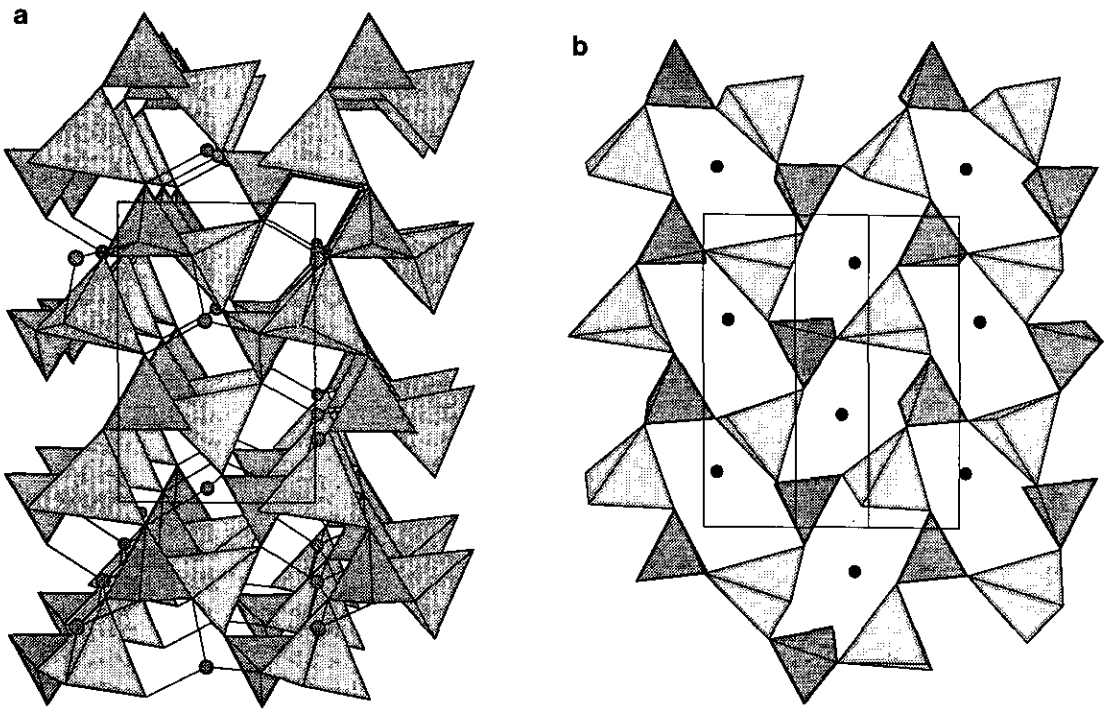

FIG. 3. (a) Perspective view of the framework structure of δ_I-$LiZnPO_4$ along [010]. (b) The pseudo-hexagonal net in the structure of δ_I-$LiZnPO_4$. Lithium is shown as spheres, PO_4 as dark-shaded tetrahedra, and ZnO_4 as light-shaded tetrahedra.

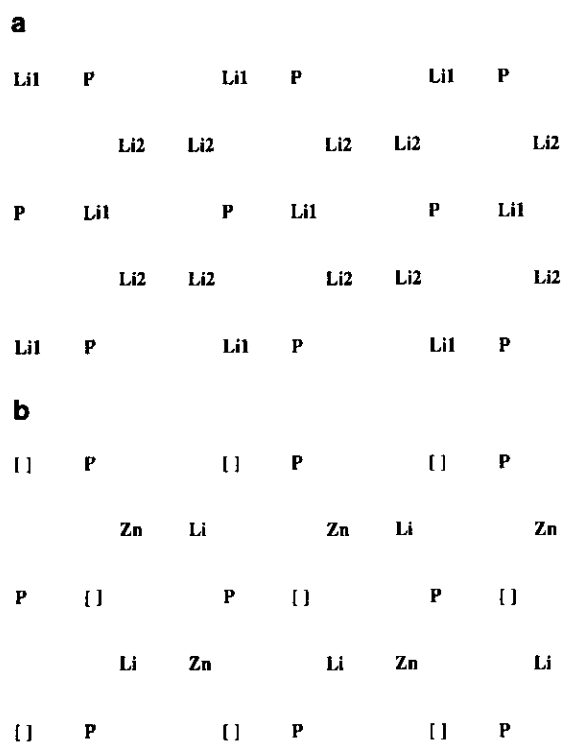

FIG. 4. A comparison between the arrangement of cations in (a) γ-Li_3PO_4 and (b) δ_I-$LiZnPO_4$.

The structure of δ_I-$LiZnPO_4$ is closely related to the structure of γ-Li_3PO_4 (20), obtained by removing one-fourth of the cations from the tetrahedral holes in the latter. Comparing the δ_I-$LiZnPO_4$ and γ-Li_3PO_4 (20) structures it is seen that the P and O positions are similar. The eight-fold Li(2) position in γ-Li_3PO_4 (*Pnam*) splits up into two fourfold positions upon going to the subgroup $Pna2_1$. Li and Zn is situated at the Li(2) position, and the Li(1) position is empty in the structure of δ_I-$LiZnPO_4$. A comparison between the cation distribution in γ-Li_3PO_4 and δ_I-$LiZnPO_4$ is given in Fig. 4.

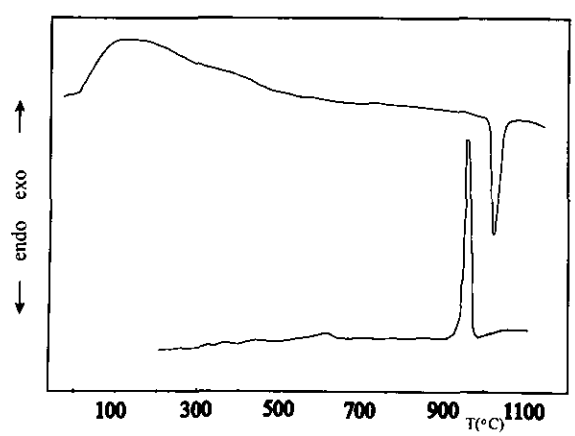

FIG. 5. Differential thermal analysis curve for δ_I-$LiZnPO_4$, heated in N_2 from RT to 1150°C. Upper curve is heating and lower is cooling.

Thermal Transformation

The HT-PXD film shows phase transitions at ~575 and ~730°C. These two transformations are not detected by the DTA experiment, Fig. 5, but are clearly visible on the Guinier Simon film. The transformation at ~575°C is characterized by some disappearing lines in the powder pattern which could indicate an order/disorder transformation. The new phase is named δ_{II}-$LiZnPO_4$. The similarity of the powder diagrams of δ_I- and δ_{II}-$LiZnPO_4$ indicates that they have essential structural elements in common. Table 6 show indexed powder diffraction patterns measured from the HT-PXD film at ~538 (δ_I) and ~632°C (δ_{II}). Further investigation of the phase transition is in progress.

TABLE 6

Guinier Simon Film Data at 538 and 632°C, Showing the Change in the Powder Profile Caused by the Phase Transition: δ_I-$LiZnPO_4$ → δ_{II}-$LiZnPO_4$

δ_I-$LiZnPO_4$ (538°C)					δ_{II}-$LiZnPO_4$ (632°C)				
h	*k*	*l*	d_{calc}	d_{obs}	*h*	*k*	*l*	d_{calc}	d_{obs}
2	0	0	5.0368	5.0391	2	0	0	5.0493	5.0747
2	0	1	4.0269	4.0276	2	0	1	4.0347	4.0322[a]
0	1	1	4.0040	4.0022	0	1	1	4.0078	4.0071[a]
1	1	1	3.7208	3.7175	1	1	1	3.7252	3.7285
2	1	0	3.5457	3.5443	2	1	0	3.5517	3.5490
0	0	2	3.3520	3.3501	0	0	2	3.3553	3.3553
2	1	1	3.1343	3.1341	2	1	1	3.1391	3.1395
2	0	2	2.7905	2.7898	2	0	2	2.7946	2.7943[a]
1	1	2	2.6824	2.6827	1	1	2	2.6853	2.6874
3	1	1	2.5729	2.5697	3	1	1	2.5776	2.5760
4	0	0	2.5184	2.5188	4	0	0	2.5246	2.5249
0	2	0	2.4961	2.4955	0	2	0	2.4984	2.5000[a]
2	1	2	2.4358	2.4356	2	1	2	2.4390	2.4369
4	0	1	2.3575	2.3575					
1	2	1	2.2786	2.2796					
3	1	2	2.1427	2.1406	3	1	2	2.1461	2.1466
4	1	1	2.1318	2.1323					
2	2	1	2.1216	2.1212					
2	0	3	2.0427	2.0424					
0	2	2	2.0020	1.9996	0	2	2	2.0039	2.0033
1	2	2	1.9636	1.9650	1	2	2	1.9656	1.9673
3	2	1	1.9194	1.9212					
2	1	3	1.8905	1.8908	2	1	3	1.8928	1.8935
2	2	2	1.8604	1.8615	2	2	2	1.8626	1.8631
4	2	0	1.7728	1.7735	4	2	0	1.7758	1.7765
0	0	4	1.6760	1.6780	0	0	4	1.6777	1.6777
6	1	1	1.5483	1.5480					
2	1	4	1.5153	1.5159	2	1	4	1.5169	1.5172
6	0	2	1.5012	1.5016					
3	3	0	1.4910	1.4914	3	3	0	1.4929	1.4935
1	3	2	1.4744	1.4752	1	3	2	1.4759	1.4753[a]
3	3	1	1.4554	1.4553	3	3	1	1.4572	1.4559
5	2	2	1.4201	1.4201	5	2	2	1.4225	1.4219
1	2	4	1.3784	1.3772	1	2	4	1.3797	1.3796
3	3	2	1.3623	1.3616	3	3	2	1.3639	1.3645
4	1	4	1.3438	1.3434	4	1	4	1.3457	1.3453
a = 10.074(3) Å					a = 10.099(5) Å				
b = 4.992(1) Å					b = 4.997(1) Å				
c = 6.704(2) Å					c = 6.711(2) Å				
36 reflections used					28 reflections used				
Cell volume = 337.1(1) Å^3					Cell volume = 338.6(2) Å^3				

[a] Lines that are unbroken on the Guinier Simon film, i.e., continue through the phase transitions: δ_I-$LiZnPO_4$ → δ_{II}-$LiZnPO_4$ → β-$LiZnPO_4$.

At ~730°C a new diffraction pattern is observed, provided in Table 7. It has not yet been possible to index the powder pattern. A reversible phase transition at higher temperature is seen in the DTA measurement (Fig. 5), at ~1003 and ~970°C (on heating and cooling, respectively). The transition temperatures given are the onset of the phase transformation. The phase transformations at ~730 and ~1003°C resemble the transformation from α- to β-$LiZnPO_4$ and from β- to γ-$LiZnPO_4$ shown in the phase diagram given by Torres-Trevino and West (2). It seems likely that δ_I-$LiZnPO_4$ is a metastabile phase, which upon heating transforms into β-$LiZnPO_4$. However, no powder patterns were given for β- and γ-$LiZnPO_4$. Schematically the thermal transformations can be presented in the following way (assuming the transformation products to be β- and γ-$LiZnPO_4$):

$$\delta_I \xleftarrow{\sim 575^\circ C} \delta_{II} \xrightarrow{\sim 730^\circ C} \beta(?) \xleftarrow{\sim 1003^\circ C} \gamma(?)\text{-}LiZnPO_4.$$

Torres-Trevino and West (2) found the following transition temperatures (reconfirmed by Elammari and Elouadi (3)),

$$\alpha \xleftarrow{\sim 737^\circ C} \beta \xleftarrow{\sim 1006^\circ C} \gamma\text{-}LiZnPO_4 \xleftarrow{\sim 1172^\circ C} (\text{liquid}),$$

where γ-$LiZnPO_4$ is proposed to exist as a solid solution, with a broad existence interval, and the ideal composition γ-$Li_4Zn(PO_4)_2$ (2). The phase transition at ~737°C was found to give a weak DTA signal (2). No structural infor-

TABLE 7

Guinier Simon Film Data (25 Reflections) of β-$LiZnPO_4$, at 840°C

d_{obs}	d_{obs}	d_{obs}
4.072 s	2.606 w	1.547 vw
4.051 vs	2.505 s	1.503 vw
4.020 vs	2.482 w	1.483 vw
3.659 m	2.462 m	1.437 vw
3.576 w	2.045 vw	1.421 vw
3.487 w	2.002 vw	1.321 vw
3.222 m	1.851 vw	1.304 vw
3.207 m	1.633.vw	
2.822 s	1.561 vw	

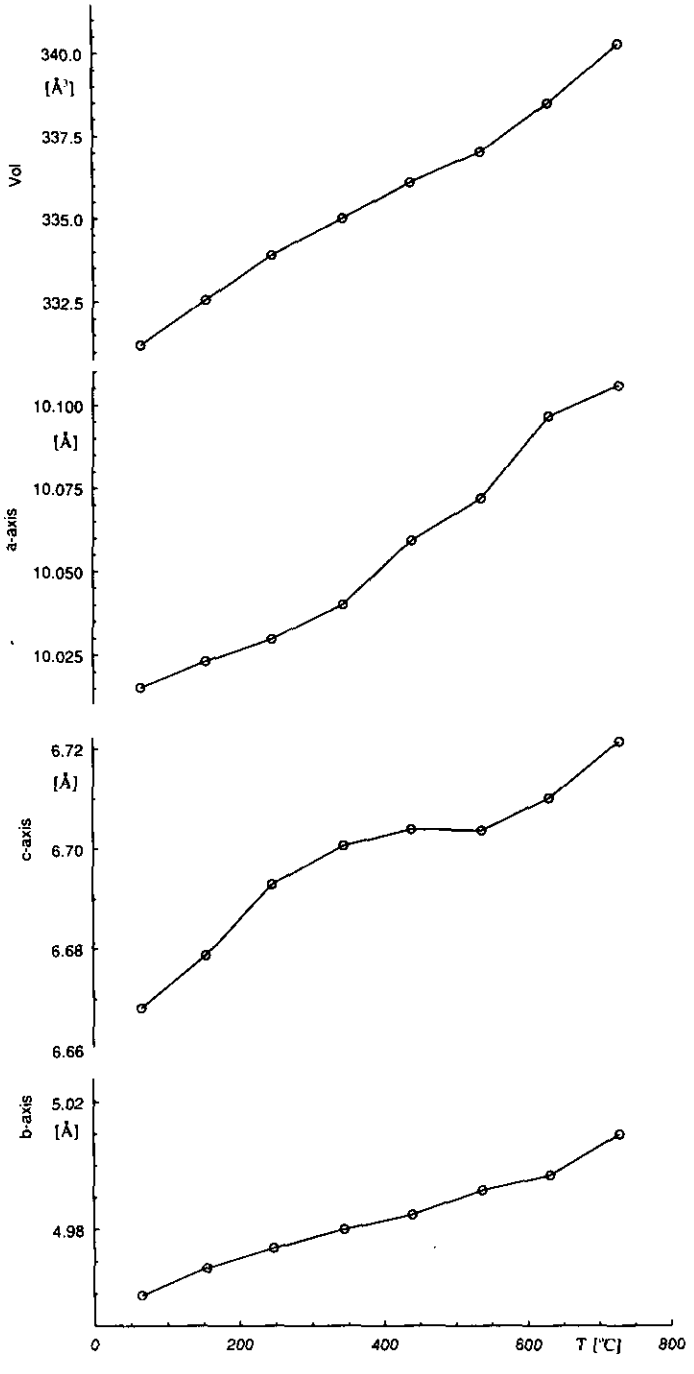

FIG. 6. Temperature dependence of the unit cell dimensions of δ_I-$LiZnPO_4$ from RT to ~575°C and of δ_{II}-$LiZnPO_4$ from ~575 to 730°C.

mation on β- and γ-$LiZnPO_4$ has been published. Table 7 provides a powder diagram (23 reflections) of what is presumably β-$LiZnPO_4$, measured from a Guinier Simon film at ~840°C.

By heating samples of δ_I-$LiZnPO_4$ at 630°C for 30 min, the phase transition to δ_{II}-$LiZnPO_4$ was found to be reversible. After heating to 950°C the compound reverts to α-$LiZnPO_4$ on cooling.

Figure 6 shows that δ_I-$LiZnPO_4$ displays almost normal thermal expansion. The linear volume expansion coefficient is $\alpha_v(\delta_I) = (1/V_0)\ (\Delta V/\Delta T) = 3.8 \times 10^{-5}\ K^{-1}$, between RT and ~575°C ($V_0(\delta_I) = 330.6(3)$ Å^3 is the estimated unit cell volume at 0°C). A significant change in the unit cell expansion is observed at the phase transition, $\delta_I \rightarrow \delta_{II}$; $\alpha_V(\delta_{II}) = 5.2 \times 10^{-5}\ K^{-1}$, between ~575 and ~730°C ($V_0(\delta_{II}) = 328.0(1)$ Å^3).

ACKNOWLEDGMENTS

Professor H. Fjellvåg, Mr. P. Fostervoll, and Mrs. K. Bjerkelund are thanked for the high temperature PXD measurements and the differential thermal analysis.

REFERENCES

1. T. E. Gier and G. D. Stucky, *Nature* **349,** 508 (1991).
2. G. Torres-Trevino and A. R. West, *J. Solid State Chem.* **61,** 56 (1986).
3. L. Elammari and B. Elouadi, *Acta. Crystallogr. Sect. C.* **45,** 1864 (1989).
4. T. R. Jensen, P. Norby, and J. Hanson, to appear.
5. P.-E. Werner, L. Eriksson, and M. Westdahl, *J. Appl. Crystallogr.* **18,** 367 (1985).
6. N. O. Ersson, "Program CELLKANT." Chemical Institute, Uppsala University, Uppsala, Sweden, 1981.
7. R. J. Cernik, P. K. Murray, P. Pattison, and A. N. Fitch, *J. Appl. Crystallogr.* **23,** 292 (1990).
8. S. P. Collins, R. J. Cernik, P. Pattison, A. M. T. Bell, and A. N. Fitch, *Rev. Sci. Instrum.* **63**(1), 1013 (1992).
9. "International Tables for X-ray Crystallography (III)." The Kynoch Press, Birmingham, England, 1962.
10. C. Keffer, A. Mighell, F. Mauer, H. Swanson, and S. Block, *Inorg. Chem.* **6,** 119 (1967).
11. J. Als-Nielsen, N. H. Andersen, C. Broholm, K. N. Clausen, and B. Lebech, The multidetector powder neutron diffractometer at Risø National Laboratory, Risø M-2720, Risø, Denmark, June 1988.
12. G. S. Pawley, *J. Appl. Crystallogr.* **14,** 357 (1981).
13. G. M. Sheldrick, C. Krüger and R. Goddard, "*Crystallographic Computing 3.*" Oxford University Press, Oxford, 1985.
14. Ch. Baerlocher, "The XRS-82 System." Institut für Kristallographie und Petrographie, ETH, Zürich, 1982.
15. D. T. Cromer, *J. Appl. Crystallogr.* **16,** 437 (1983).
16. H. J. Jakobsen, P. Daugaard and V. Langer, *J. Magn. Reson.* **76,** 162 (1988).
17. P. Norby, *Zeolites* **10,** 193 (1990).
18. I. D. Brown and D. Altermatt, *Acta Crystallogr. Sect. B* **41,** 244 (1985).
19. T. F. W. Barth and E. Posnjak, *Z. Kristallogr.* **81,** 135 (1932).
20. J. Von Zemann, *Acta Crystallogr.* **13,** 863 (1960).